Expressway deformation mapping using high-resolution TerraSAR-X images

Article *in* Remote Sensing Letters · January 2014

DOI: 10.1080/2150704X.2014.891774

CITATIONS
14

READS
153

5 authors, including:

Xuguo Shi
China University of Geosciences
29 PUBLICATIONS **155** CITATIONS
SEE PROFILE

Jian Wang
Southwest Normal University
1,388 PUBLICATIONS **15,076** CITATIONS
SEE PROFILE

Min Zhang
Beijing University of Posts and Telecommunications
888 PUBLICATIONS **5,685** CITATIONS
SEE PROFILE

Wei Shan
Northeast Forestry University
102 PUBLICATIONS **226** CITATIONS
SEE PROFILE

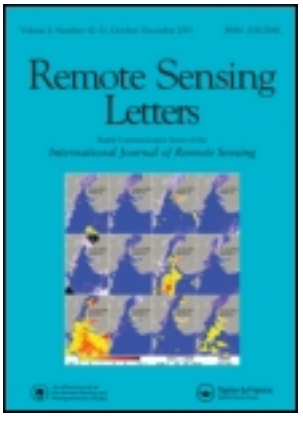

Remote Sensing Letters
Publication details, including instructions for authors and subscription information:
http://www.tandfonline.com/loi/trsl20

Expressway deformation mapping using high-resolution TerraSAR-X images

Xuguo Shi[a], Mingsheng Liao[a], Teng Wang[b], Lu Zhang[a], Wei Shan[c] & Chunjiao Wang[c]

[a] State Key Laboratory of Information Engineering in Surveying, Mapping and Remote Sensing, Wuhan University, Wuhan, P.R. China

[b] Division of Physical Sciences and Engineering, King Abdullah University of Science and Technology, Thuwal, Saudi Arabia

[c] Engineering Consulting and Design Institute, Northeast Forestry University, Harbin, P.R. China

Published online: 07 Mar 2014.

To cite this article: Xuguo Shi, Mingsheng Liao, Teng Wang, Lu Zhang, Wei Shan & Chunjiao Wang (2014) Expressway deformation mapping using high-resolution TerraSAR-X images, Remote Sensing Letters, 5:2, 194-203, DOI: 10.1080/2150704X.2014.891774

To link to this article: http://dx.doi.org/10.1080/2150704X.2014.891774

Remote Sensing Letters, 2014
Vol. 5, No. 2, 194–203, http://dx.doi.org/10.1080/2150704X.2014.891774

Taylor & Francis
Taylor & Francis Group

Expressway deformation mapping using high-resolution TerraSAR-X images

Xuguo Shi[a], Mingsheng Liao[a], Teng Wang[b], Lu Zhang[a]*, Wei Shan[c], and Chunjiao Wang[c]

[a]*State Key Laboratory of Information Engineering in Surveying, Mapping and Remote Sensing, Wuhan University, Wuhan, P.R. China;* [b]*Division of Physical Sciences and Engineering, King Abdullah University of Science and Technology, Thuwal, Saudi Arabia;* [c]*Engineering Consulting and Design Institute, Northeast Forestry University, Harbin, P.R. China*

(*Received 22 November 2013; accepted 30 January 2014*)

Monitoring deformation of linear infrastructures such as expressway and railway caused by natural processes or anthropogenic activities is a vital task to ensure the safety of human lives and properties. Interferometric Synthetic Aperture Radar (InSAR) has been widely recognized as an effective technology to carry out large-area surface deformation mapping. However, its application in linear infrastructure deformation monitoring has not been intensively studied till now. In this article, a modified Small BAseline Subset (SBAS) method is proposed to retrieve the deformation patterns of the expressway. In our method, only the point-like targets identified on the expressway were kept in our analysis, and two complementary subsets of interferograms were formed to better separate the signals of height error and deformation from inteferometric phase observations. We successfully applied this method with multitemporal high-resolution TerraSAR-X images to retrieve the spatial-temporal pattern of surface deformation along the Bei'an-Heihe expressway that is located in island-permafrost areas and threatened by geohazards.

1. Introduction

Linear infrastructures such as expressway and railway are important in linking populated cities. Deformation of such infrastructures due to natural processes and anthropogenic activities will not only cut off the transportation, but also bring serious safety problems. For example, expressways in mountain areas are usually threatened by landslides and other geological hazards (Nie, Zhang, and Jian 2013). It is therefore essential to monitor the deformation of such infrastructures accurately and timely. Interferometric synthetic aperture radar (InSAR) has been widely recognized by the scientific community as an effective way for measuring deformation with its large coverage and all weather acquisition capability.

However, the practical application of InSAR is limited by temporal and spatial decorrelations, which is particularly significant in heavily vegetated mountainous areas. Permanent/persistent scatter InSAR (PSI) (Ferretti, Prati, and Rocca 2001) and Small BAseline Subset (SBAS) (Berardino et al. 2002; Mora, Mallorqui, and Broquetas 2003) were proposed to overcome such limitations and have been successfully applied in many cases. Meanwhile, since the TerraSAR-X and COSMO-SkyMed satellites were launched in 2007, high-resolution SAR data have been acquired steadily. Although PSI or SBAS

*Corresponding author. Email: luzhang@whu.edu.cn

can identify more point-like targets (PTs) from high-resolution SAR data than from medium-resolution ENVISAT Advanced Synthetic Aperture Radar (ASAR) data in urban areas (Strozzi, Teatini, and Tosi 2009), the short wavelength of X-band makes the InSAR analysis suffer more from temporal decorrelation, especially in vegetated area. Only a limited number of PTs could be identified using PSI or traditional SBAS in vegetated mountainous area, which will result in unreliable deformation mapping.

In this letter, we first describe a modified SBAS method for linear infrastructure deformation mapping. Then, the proposed method was applied to obtain the time-series deformation trend of the Bei'an-Heihe expressway in Northeastern China with high-resolution TerraSAR-X data.

2. Deformation estimation on linear infrastructures

2.1. Point-like target detection

X-band SAR interferometry heavily suffers from temporal and spatial decorrelation in mountainous areas covered by dense vegetation (Bovenga et al. 2012). Fortunately, man-made linear infrastructures like expressways built in such areas usually maintain good coherence over a long time span due to its stable backscattering. However, few PTs can be detected in the vicinity. Instead of improving point density in the surrounding areas, here we will focus on the PTs associated with the expressway. In other words, only PTs on the expressway are extracted and processed in the time-series analysis.

We adopted the amplitude dispersion index as the criteria to select PT candidates (Ferretti, Prati, and Rocca 2001). A loose threshold can be set initially to make sure that more points could be chosen as candidates. PTs are manually deleted if they are obviously not on the expressway. We only kept the PTs with the minimum amplitude dispersion value in each line (or sample) along the expressway. Then, the following procedure of phase unwrapping could be reduced to a one-dimensional problem.

It is natural to assume that slow deformation and topographic errors are generally spatially correlated as a regional phenomenon and will not concentrate on just one point. Therefore, the phase difference between two adjacent pixels along the expressway should be within the range $(-\pi, \pi]$, if a high density of PTs along the expressway is obtained. This assumption is critical to the one-dimensional phase unwrapping. Usually, it is valid for most of the slow-moving targets observed by satellite SAR systems with both high spatial resolution and short repeat cycle.

2.2. Phase composition of point-like targets

The differential phase $\Delta\phi_{\mathrm{dif}}$ on the detected PTs can be regarded as the summation of four components with respect to a given reference point as below (Mora, Mallorqui, and Broquetas 2003):

$$\Delta\phi_{\mathrm{dif}} = \Delta\phi_{\mathrm{mov}} + \Delta\phi_{\mathrm{topo}} + \Delta\phi_{\mathrm{atm}} + \Delta\phi_{\mathrm{n}} \tag{1}$$

where $\Delta\phi_{\mathrm{mov}}$ denotes the phase change due to movement of the PT in the satellite line-of-sight (LOS) direction, $\Delta\phi_{\mathrm{topo}}$ denotes the residue topographic phase due to the inaccurate DEM, $\Delta\phi_{\mathrm{atm}}$ denotes the phase caused by atmospheric path delay variation between two passes and $\Delta\phi_{\mathrm{n}}$ is the noise term. The deformation phase component can be expressed as:

$$\Delta\phi_{\text{mov}} = tv_{\text{ln}} + \Delta\phi_{\text{nl}} \tag{2}$$

where t is the temporal baseline of the interferogram, v_{ln} is the linear deformation rate and $\Delta\phi_{\text{nl}}$ is the non-linear deformation phase.

The residual topographic phase $\Delta\phi_{\text{topo}}$ depends on the normal baseline B and the height error Δh as well as on radar wavelength λ, slant range R and incidence angle θ as below:

$$\Delta\phi_{\text{topo}} = \frac{4\pi}{\lambda}\frac{B}{R\sin\theta}\Delta h \tag{3}$$

2.3. Phase unwrapping

The differential phase in Equation (1) must be unwrapped and decomposed to separate deformation signal from other phase components. The phase unwrapping is a one-dimensional problem following PT detection in our method, and thus traditional 2D phase unwrapping can be avoided. With the assumption on phase pattern in Section 2.1, the unwrapped phase can be achieved by just subtracting/adding only one cycle, i.e. 2π from/to the wrapped phases when phase jump appears. In particular, if the phase difference between two adjacent PTs P_1 and P_2 $\phi_{P_1} - \phi_{P_2} \leq -\pi$, 2π will be subtracted from the phase of P_2 to obtain the unwrapped phase, while when the difference $\phi_{P_1} - \phi_{P_2} > \pi$, 2π will be added to the phase of P_2. Nevertheless, this approach may fail when applied to more problematic test sites, e.g. areas characterized by abrupt phase change, for which artificial one-dimensional phase unwrapping can be employed to avoid the failure.

2.4. Deformation retrieval

The global Shuttle Radar Topography Mission (SRTM) DEM of 3 arc-second resolution (approximate 90 m) was produced in February 2000. Such a resolution is too coarse for processing TerraSAR-X data of 3 m or 1 m resolution. Although the vertical error of the SRTM DEM has been declared to be less than 16 m, it has been more than 10 years since the mission and the earth surface might have changed in various regions. Hence, the SRTM DEM must be used cautiously especially in rapidly developing countries like China (Perissin and Teng 2011). Moreover, differential InSAR with X-band data is more sensitive to height errors and slow deformation (Bovenga et al. 2012). Therefore, accurate estimation of height error and deformation signal becomes more crucial when dealing with slowly deforming targets.

Here, in order to effectively separate height error from deformation signal, the interferograms formed with $N + 1$ SAR images acquired from time t_0 to time t_N are grouped into a DEM subset and a deformation subset. The DEM subset consists of M_{T} interferograms with short temporal baselines and moderate normal baselines. The deformation subset used to effectively estimate deformation phase signals is comprised of M_{D} interferograms with long temporal baselines and short normal baselines. Then, we estimate height error and linear deformation rate from the DEM subset and deformation subset in an iterative procedure, which is elaborated as follows.

For the DEM subset, Equation (1) can be expressed as

$$\begin{cases} \Delta\phi_{\text{dif}} = [\mathbf{T} \quad \mathbf{P}][\begin{matrix} v \\ \Delta h \end{matrix}] + \Delta\phi_{\text{N}} \\ \Delta\phi_{\text{N}} = \Delta\phi_{\text{nl}} + \Delta\phi_{\text{atm}} + \Delta\phi_{\text{n}} \end{cases} \tag{4}$$

where $\mathbf{T} = [t_1 \ldots t_{M^T}]^{\text{T}}$, $\mathbf{P} = [p_1 \ldots p_{M^T}]^{\text{T}}$, t_i is the temporal baseline and $p_i = \frac{4\pi}{\lambda}\frac{B_i}{R_i \sin\theta_i}$ is the change rate of phase with respect to height for the ith ($i = 1, \ldots, M^T$) interferogram as defined in Equations (2) and (3). A two-dimensional regression is first applied to retrieve an initial estimation of height error Δh and linear deformation rate v. Then, the estimated height error was removed from the deformation subset and we can obtain the residual phase $\delta\phi_{\text{res}}$

$$\delta\phi_{\text{res}} = \Delta\phi_{\text{dif}} - \Delta\phi_{\text{topo}} = tv + \Delta\phi_{\text{nl}} + \Delta\phi_{\text{atm}} + \delta\phi_{\text{n}} \tag{5}$$

For the deformation subset, Equation (5) can be expressed as

$$\begin{cases} \delta\phi_{\text{res}} = \mathbf{T}v + \delta\phi_{\text{N}} \\ \delta\phi_{\text{N}} = \Delta\phi_{\text{nl}} + \Delta\phi_{\text{atm}} + \delta\phi_{\text{n}} \end{cases} \tag{6}$$

where $\boldsymbol{T} = [t_1 \ldots t_{M_T}]^{\text{T}}$. The updated linear deformation rate v was retrieved using a least-square regression procedure from the deformation subset.

The linear deformation rate estimated from the deformation subset was then substituted into Equation (4), and the deformation phase can be removed from the differential phase of the DEM subset. Then, Equation (4) becomes the following form:

$$\begin{cases} \Delta\phi_{\text{dif}} - \mathbf{T}v = \mathbf{P}\Delta h + \Delta\phi_{\text{N}} \\ \Delta\phi_{\text{N}} = \Delta\phi_{\text{nl}} + \Delta\phi_{\text{atm}} + \Delta\phi_{\text{n}} \end{cases} \tag{7}$$

The height error was also estimated using a least-square regression from the DEM subset. Using such an iterative processing strategy, estimation of height error and linear deformation rate can be refined gradually from the DEM subset and the deformation subset with Equations (6) and (7). The iteration will not be terminated until the variations of estimates are lower than a predefined threshold.

The estimated height error and linear deformation signal are finally removed from the deformation subset. Afterwards, our focus turned to the retrieval of non-linear deformation series from the residual phase in the deformation subset. Atmospheric phase cannot be neglected in time-series processing. Although a one-dimensional phase unwrapping is performed in our method, actually the points have a two-dimensional distribution. To separate the atmospheric phase and the non-linear deformation phase, a two-dimensional filter is preferred. But we can hold that the atmospheric condition is homogeneous within a limited distance, a one-dimensional fifth order Butterworth low-pass filter with selected window length in space and a triangular filter in time domain are applied on the residual to isolate the atmospheric phase (Ferretti, Prati, and Rocca 2001). Then the atmospheric phase can be removed from the deformation subset phase residuals. The residuals after atmospheric phase removal could be expressed as follows:

$$\delta\phi_{\text{res}} = \Delta\phi_{\text{dif}} - \Delta\phi_{\text{topo}} - tv - \Delta\phi_{atm} = \delta\phi_{nl} + \delta\phi_{n} = B\mathbf{V}_{nl} + \delta\phi_{n} \tag{8}$$

V_{n1} is the non-linear deformation velocity vector $[v_1 \ldots v_N]$. Matrix $\boldsymbol{B}$ is a matrix of size $M_D \times N$; the generic element (m, k) is defined as $\boldsymbol{B}(m, k) = t_{k+1} - t_k$ for $i + 1 \le k \le j$, $\forall m = 1,$

…,M_D and $\boldsymbol{B}(m, k) = 0$ elsewhere. Here i, j are the indexes of master image and slave image, $0 \le i < j \le N$ and t_k is the element of $\mathbf{T}$ in Equation (6). Then the non-linear deformation rate was retrieved by singular value decomposition (SVD) in case that matrix $\boldsymbol{B}$ is rank defect (Berardino et al. 2002; Mora, Mallorqui, and Broquetas 2003). Assuming the deformation of all the points as zero at the first acquisition date, we can obtain the time-series deformation as follows.

$$d_i = -\frac{4\pi}{\lambda}\sum_{k=1}^{i}(t_{k+1} - t_k)v_k - \frac{4\pi}{\lambda}(t_i - t_0)v \tag{9}$$

i denotes the index of SAR images, $0 \le i \le N$. d_i is the corresponding non-linear deformation, v_k is kth element of $\mathbf{V}_{\mathrm{nl}}$ in Equation (8), while v is the linear deformation rate in Equation (2).

A detailed workflow of the modified small-baseline time-series SAR interferometric analysis method is given in Figure 1.

3. Experimental results and analyses

The Bei'an-Heihe expressway linking Bei'an County and Heihe City is an indispensable part of China's national highway network. It was initially built as a national highway around 2000 and then upgraded to expressway since 2009 (Shan, Jiang, and Cui 2012).

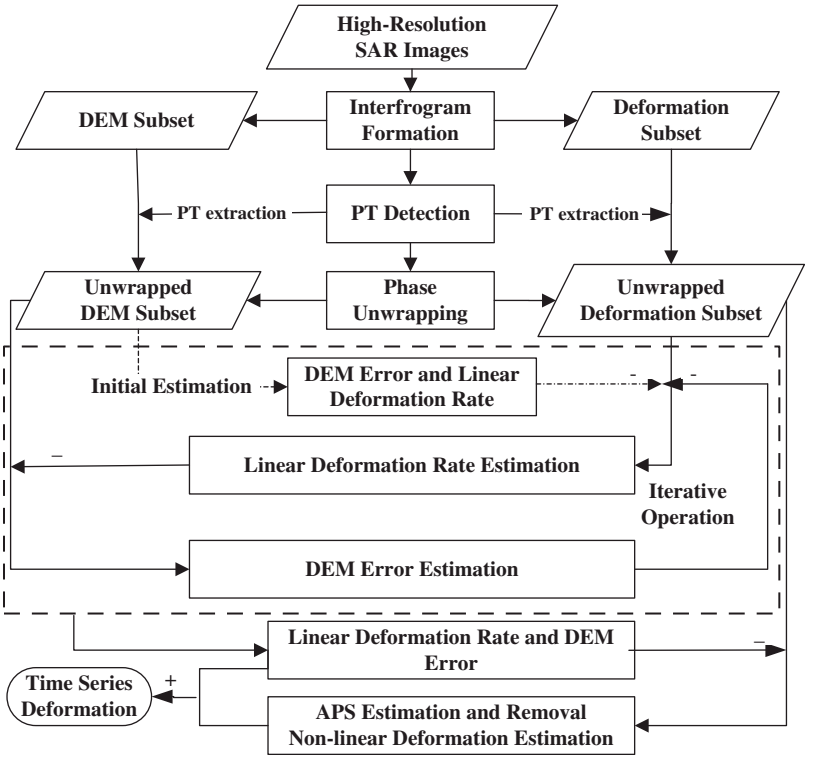

Figure 1. Workflow of modified Small BAseline Subset (SBAS) method.

This expressway with four lanes of width being 3.75 m covered with asphalt concrete pavement is an important transportation channel for the northern border region leading to inner Heilongjiang province. Constructions built on permafrost or seasonally frozen soils suffer from the annual cycle of freezing and thawing activity. The situation became more complicated after the expressway expansion project in 2009. Some sections of the expressway were built on island permafrost within the central Lesser Khingan Mountain area and some sections were even located on landslides (Shan, Wang, and Hu 2012). Landslide occurred made part of the expressway lose stability and have to change route finally (Shan, Wang, and Hu 2012). A part of the expressway threatened by permafrost and landslide located near Sunwu County is chosen as our study area, outlined by the red rectangle that is shown in Figure 2(*a*).

Since the Lesser Khingan Mountain areas are usually covered by snow, a data set of 12 descending TerraSAR-X images in HH polarization and Stripmap-mode, acquired from May to November of 2012 was used to generate 40 interferograms. The SRTM DEM of 3 arc-second resolution covering this area was used to remove the topographic phase. Thirteen interferograms with normal baselines less than 300 m and temporal baseline less than 1 month were grouped as the DEM subset to estimate height error. The other 27 interferograms with normal baselines less than 100 m and temporal baseline longer than 1 month formed the deformation subset that was used to extract deformation information. Distributions of acquisition date and normal baseline of interferograms in the two subsets are plotted in Figure 2(*b*).

3.1. *Mean velocity of deformation*

In our test site, no *in situ* measurement data are available for performing validation till now. Therefore, a point located at the highest place and outside the geological hazard zones was chosen as a stable reference to carry out result calibration. The location of the

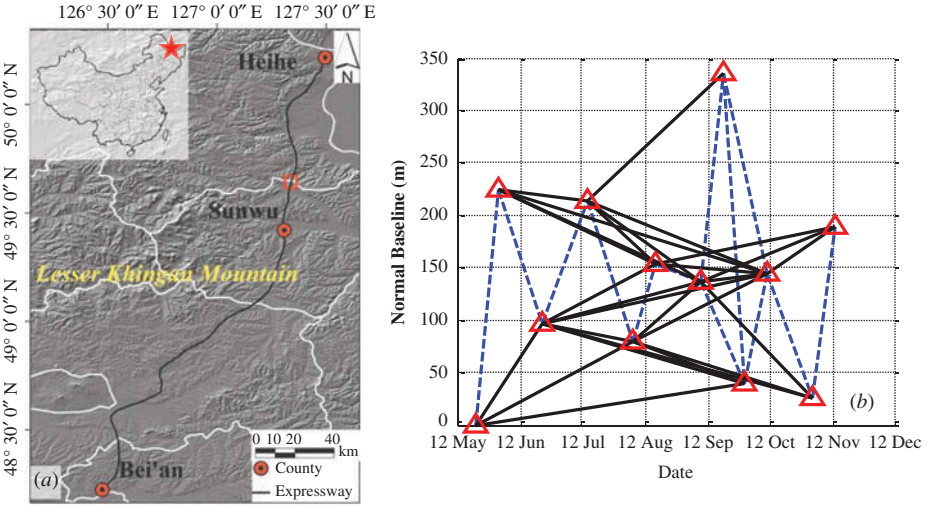

Figure 2. (*a*) Location of Bei'an-Heihe expressway. The red rectangle represents our study area. (*b*) Spatial-temporal baseline plot of the TerraSAR-X interferograms. The red triangles represent SAR images, while dashed blue lines and solid black lines indicate interferograms in the DEM subset and the deformation subset, respectively.

reference point is marked by the red cross in Figure 3. Figure 3(*a*) shows the estimated height error. A section of the expressway identified by the yellow arrow in Figure 3(*a*) has been abandoned due to severe damage (Shan, Jiang, and Cui 2012), and a new section marked by the white arrow was built to replace the old one. Consequently, the height error over the newly built section is relatively higher than other places along the expressway. Since the SRTM DEM was obtained in 2000 and the new section was built after 2009, the height error of this section actually indicates the basement of the newly built section, which demonstrated the reliability of our method to a certain extent.

Figure 3(*b*) shows the estimated mean LOS deformation velocity along the expressway. From the result, we can see that the section P suffers most severely from deformation. This part of expressway lies on discontinuous island permafrost zones, and the annual cycle of permafrost freezing and thawing will lead to serious land surface deformation. Besides the permafrost, L1, L2, L3 and L4 in Figure 3(*b*) represent four landslides in our study area. PTs around L1, L2 and L3 showed a relatively active deforming trend, nearly from –2 cm year^{-1} to –1 cm year^{-1}. The newly built part of the expressway was overall stable, except at a few points around L4. I1-I2 in Figure 3(*b*) is the intersection area between the old and the newly built parts of the expressway. We identified an active deformation trend of about –2 cm year^{-1} in this area. Meanwhile, S indicates three spots identified on the southern part of expressway suffering from

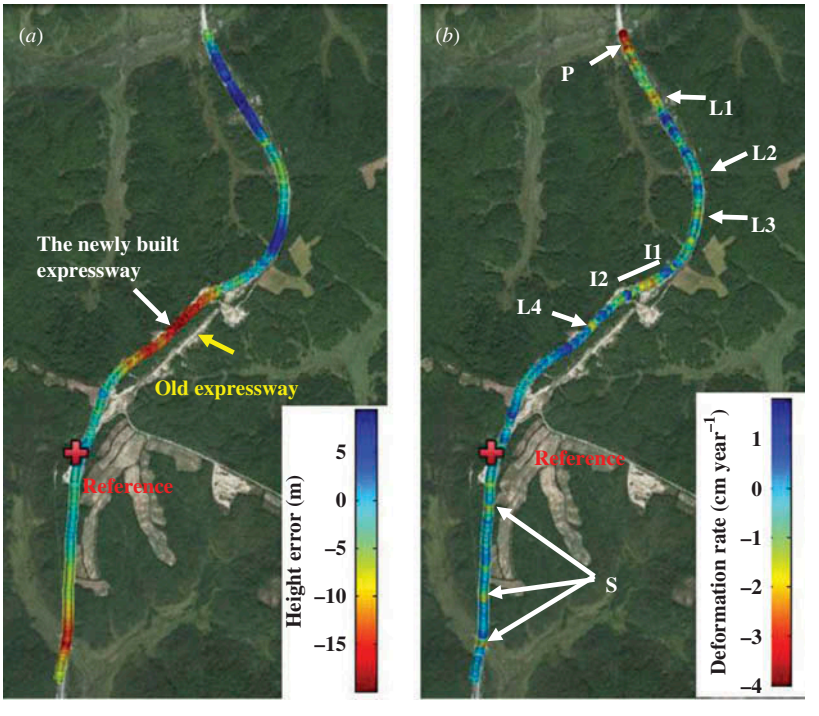

Figure 3. (*a*) Estimated height error. The red cross represents the location of the reference points used in our process. (*b*) Measured line-of-sight (LOS) deformation rate. P represents discontinuous permafrost area. L1, L2, L3 and L4 represent different landslides along the expressway. I1-I2 represents the intersection between the old expressway and the newly built expressway. S represents three spots where deformations were identified on the expressway. Background image: Google Earth™.

deformation of about –2 cm year^{-1} with respect to the reference point. Since it is down slope from L4 to S, the water supplies including rainfall and frozen soil melting at the area S are more adequate. We also found from Google Earth that these three spots were relatively lower areas that provide places for water storage. These two factors will soften the local roadbed so as to significantly increase the possibility of subsidence at the three spots (Ma et al. 2011).

3.2. *Time-series deformation analysis*

Time-series deformation tendencies around the intersection I1-I2 marked in Figure 3(*b*) are shown in Figure 4. Obvious deformation was observed in this area. Since the expressway is built on seasonally frozen soils, the increasing temperature makes the ice in the soil melt, leading to a soft subgrade. The deformation of the expressway was a bit larger from May to early July caused by the soil thawing. Furthermore, landslide occurred made the old expressway shown in Figure 3(*b*) lose stability (Shan, Wang, and Hu 2012). The movement of landslide might also make the subgrade of this area unstable.

A PT identified within the permafrost area is chosen as a representative to qualitatively evaluate the impacts of changing weather conditions on the stability of the expressway in this study. The location of this point is marked by P in Figure 3(*b*). The time series of LOS

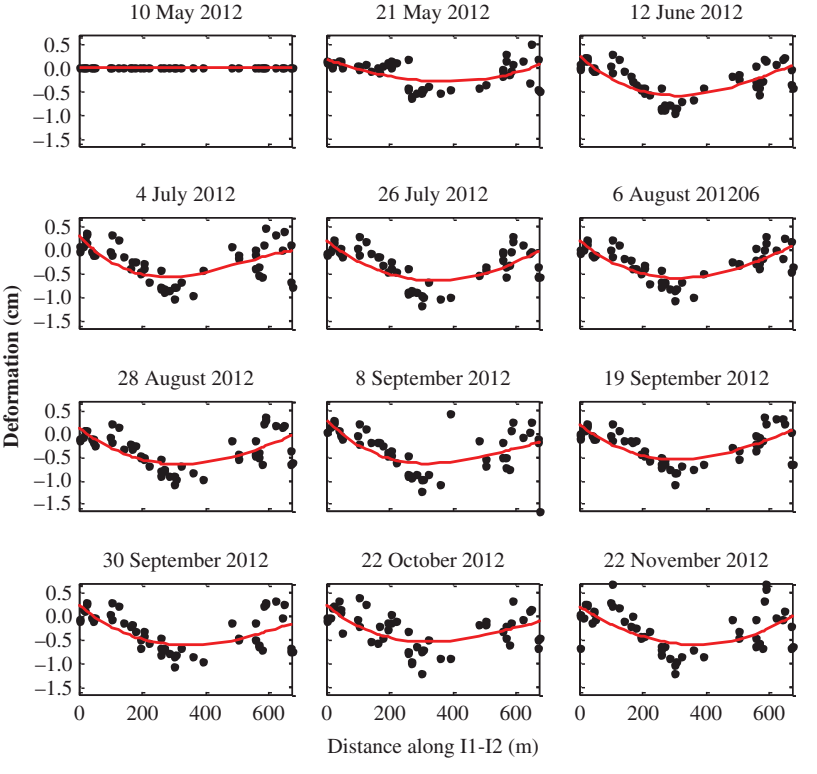

Figure 4. Time-series deformation of I1-I2 on the expressway. I1-I2 is the intersection marked in Figure 3(*b*). All the deformation is relatively to the first scene obtained on 10 May 2012. Each black dot represents a point-like target on the expressway. The estimated tendencies represented by the red lines are given in each scene.

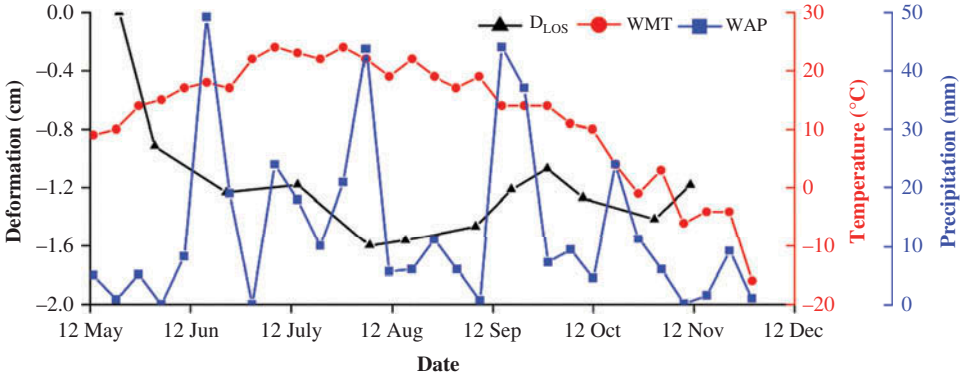

Figure 5. Time-series deformation of P on the expressway is plotted along with weekly mean temperature (WMT) and weekly accumulative precipitation (WAP) (The Weather Channel Companies 2012).

deformation at this point together with weekly mean temperature and weekly accumulative precipitation is plotted in Figure 5. Generally, there seems to be a good correlation between the temperature variation and the LOS deformation at point P. We can see a rapid subsidence from May to July along with the increasing temperature in early summer, and the deformation reaches a maximum of 1.6 cm in late July. This phenomenon can be principally explained by the permafrost thawing. Afterwards, the temperature decreases significantly from late July to mid-September, accompanied by uplift at point P which may be caused by frost heaving effect. By contrast, the precipitation seems to have little impact on the expressway deformation at point P. A subtle subsidence trend from mid-September to October observed in Figure 5 might be attributed to the rainfall and snowfall during this period. But in late October, when the temperatures decreased to below zero and when the snowfall was less than 10 mm, the uplift caused by frost heaving effect showed up again.

4. Conclusion

High-resolution TerraSAR-X data have been successfully used in the deformation mapping of Bei'an-Heihe expressway in Northeastern China. A modified SBAS method is first presented for linear infrastructure deformation mapping. Since high-resolution X-band interferometric SAR imaging are sensitive to height error and surface change, a DEM subset and a deformation subset were jointly analysed to iteratively separate the phase components of linear deformation and height error. The proposed method was successfully applied to retrieve spatial and temporal deformation pattern of Bei'an-Heihe expressway from a limited number of high-resolution TerraSAR-X images. Non-uniform deformation was identified at the intersection between the abandoned part of expressway and the newly built section. The application of the strategy we proposed will not only be limited to the deformation mapping of expressways, but also be applied to monitoring long-term safety of any linear infrastructures exposed on the ground that can be periodically observed by high-resolution satellite SAR sensors.

Acknowledgements

The TerraSAR-X data sets are copyrighted by DLR/Infoterra GmbH. The SRTM DEM is provided by NASA/JPL.

Funding

This work is financially supported by the National Key Basic Research Program of China [grant number 2013CB733204, 2013CB733205]; the National Natural Science Foundation of China [grant number 61331016, 41271457, 41174120, 41021061] and the Shanghai Academy of Spaceflight Technology Innovation Fund [grant number SAST201214].

References

Berardino, P., G. Fornaro, R. Lanari, and E. Sansosti. 2002. "A New Algorithm for Surface Deformation Monitoring Based on Small Baseline Differential SAR Interferograms." *IEEE Transactions on Geoscience and Remote Sensing* 40 (11): 2375–2383.

Bovenga, F., J. Wasowski, D. O. Nitti, R. Nutricato, and M. T. Chiaradia. 2012. "Using COSMO/SkyMED X-Band and ENVISAT C-Band SAR Interferometry for Landslides Analysis." *Remote Sensing of Environment* 119: 272–285.

Ferretti, A., C. Prati, and F. Rocca. 2001. "Permanent Scatterers in SAR Interferometry." *IEEE Transactions on Geoscience and Remote Sensing* 39 (1): 8–20.

Ma, W., Y. Mu, Q. Wu, Z. Sun, and Y. Liu. 2011. "Characteristics and Mechanisms of Embankment Deformation Along the Qinghai–Tibet Railway in Permafrost Regions." *Cold Regions Science and Technology* 67 (3): 178–186.

Mora, O., J. J. Mallorqui, and A. Broquetas. 2003. "Linear and Nonlinear Terrain Deformation Maps From a Reduced Set of Interferometric SAR Images." *IEEE Transactions on Geoscience and Remote Sensing* 41 (10): 2243–2253.

Nie, L., M. Zhang, and H. Jian. 2013. "Analysis of Surface Subsidence Mechanism and Regularity Under the Influence of Seism and Fault." *Natural Hazards* 66 (2): 773–780.

Perissin, D., and W. Teng. 2011. "Time-Series InSAR Applications Over Urban Areas in China." *IEEE Journal of Selected Topics in Applied Earth Observations and Remote Sensing* 4 (1): 92–100.

Shan, W., H. Jiang, and G. H. Cui. 2012. "Formation Mechanism and Characteristics of the Bei'an to Heihe Expressway K177 Landslide." *Advanced Materials Research* 422: 663–668.

Shan, W., C.-J. Wang, and Q. Hu, 2012. "Expressway and Road Area Deformation Monitoring Research Based on InSAR Technology in Isolated Permafrost Area." 2012 2nd International Conference on Remote Sensing, Environment and Transportation Engineering (RSETE), Nanjing, June 1–3.

Strozzi, T., P. Teatini, and L. Tosi. 2009. "TerraSAR-X Reveals the Impact of the Mobile Barrier Works on Venice Coastland Stability." *Remote Sensing of Environment* 113 (12): 2682–2688.

The Weather Channel Companies. 2012."Weather Underground." Accessed January 3, 2013. http://www.wunderground.com/